Broadband InGaAs-capped InAs/GaAs quantum-dot infrared photodetector with Bi-modal dot height distributions

Wei-Hsun Lin and Shih-Yen Lin

Citation: Journal of Applied Physics **112**, 034508 (2012); doi: 10.1063/1.4745052
View online: http://dx.doi.org/10.1063/1.4745052
View Table of Contents: http://scitation.aip.org/content/aip/journal/jap/112/3?ver=pdfcov
Published by the AIP Publishing

Broadband InGaAs-capped InAs/GaAs quantum-dot infrared photodetector with Bi-modal dot height distributions

Wei-Hsun Lin[1] and Shih-Yen Lin[2,3,4,a)]
[1]*Institute of Electronics Engineering, National Tsing Hua University, Hsinchu 300, Taiwan*
[2]*Research Center for Applied Sciences, Academia Sinica, Taipei 11529, Taiwan*
[3]*Department of Photonics, National Chiao-Tung University, Hsinchu 300, Taiwan*
[4]*Institute of Optoelectronic Sciences, National Taiwan Ocean University, Keelung 20224, Taiwan*

(Received 16 February 2012; accepted 17 July 2012; published online 8 August 2012)

The influence of quantum-dot (QD) height distribution on the detection wavelengths of InGaAs-capped quantum-dot infrared photodetectors (QDIPs) is investigated. For devices with 2.8 and 2.0 mono-layer (ML) InAs coverage, 7.6 and 10.4 μm detection wavelengths are observed. The results suggest that reduced dot height would result in a longer detection wavelength. By using 2.4 ML InAs QDs with bi-modal dot height distributions, a 6–12 μm broadband QDIP is achieved with the combination of $\sim$8 and $\sim$10 μm peak detection wavelengths contributed by the larger and smaller InAs QDs. © *2012 American Institute of Physics*. [http://dx.doi.org/10.1063/1.4745052]

I. INTRODUCTION

Compared with conventional quantum-well infrared photodetectors (QWIPs), quantum-dot infrared photodetectors (QDIPs) have already demonstrated advantages, including high-temperature operation[1,2] and insensitivity to incident light polarization.[3,4] QDIP focal-plane arrays for thermal imaging applications have also been demonstrated.[5,6] However, due to self assembled quantum-dots (QDs) are adopted for the device, QD size control is always a challenge for QDIPs. In this case, the detection wavelength tuning for QDIPs is not as flexible as QWIPs and for most QDIPs, the detection wavelengths are limited at the mid-wavelength infrared range (MWIR; 3–5 μm). The lack of QDIPs operated at the long-wavelength infrared range (LWIR; 8–12 μm) makes the devices incapable of multi-color and broadband detections covering both infrared ranges. To improve this disadvantage, InGaAs-capped QDIPs are proposed, which have demonstrated the capability of wavelength tuning from MW- to the LW-IR ranges.[7–9] As discussed in the previous reports, the wavelength tuning from MW- to the LW-IR ranges of the InGaAs-capped QDIPs is achieved via QD size reduction. The results have revealed the possibility of broadband detection if the QD height distribution can be broadened via changing the growth conditions.

In this paper, the influence of QD height distribution on the detection wavelengths of InGaAs-capped QDIPs is investigated. For the device with 2.8 mono-layer (ML) InAs coverage, the observed 7.6 μm detection wavelength is resulted from the dominant larger InAs QDs with average dot height/diameter 9.0/50.8 nm. For the device with 2.0 ML InAs coverage, 10.4 μm detection wavelength is observed due to the dominant smaller dot height/diameter 4.4/42.7 nm. With the combination of $\sim$8 and $\sim$10 μm detection wavelengths contributed by the larger and smaller InAs QDs, 6–12 μm broadband detection is observed for the device with 2.4 ML InAs coverage. The results have demonstrated that by simply randomizing the QD height distribution, InGaAs-capped QDIPs with broadband detection can be achieved without additional device structure design.

II. EXPERIMENTS

The samples discussed in this paper are grown on (100)-oriented semi-insulating GaAs substrates by using a Riber Compact-21 solid-source molecular beam epitaxy system. The device structures are shown in Table I. For all samples, 300 and 600 nm n-type doped GaAs layers are grown as top and bottom contacts, respectively. The active regions of the devices are ten-periods InGaAs-capped InAs/GaAs QDs, where 8 nm $In_{0.15}Ga_{0.85}As$ and 42 nm undoped GaAs layers are adopted. Three samples with 2.0, 2.8, and 2.4 ML InAs coverage are prepared, which are referred as samples A, B, and C, respectively. To investigate corresponding QD surface morphologies, additional wafers with InAs QD layers with the same growth conditions are grown on top of the GaAs layers. Standard photolithography and chemical wet etching are adopted to fabricate devices with $100 \times 100\ \mu m^2$ mesas. The spectral response measurement system consists of a Perkin Elmer spectrum 100 Fourier Transform Infrared system coupled with a cryostat and a SR-570 current-preamplifier.[7–9]

III. RESULTS AND DISCUSSIONS

The $1 \times 1\ \mu m^2$ atomic force microscopic (AFM) images of InAs QDs with the same growth conditions as samples A and B are shown in the Fig. 1(a). As shown in the figure, different QD size distributions are observed for the two samples. For sample A, smaller average dot height/diameter 4.4/42.7 nm are observed, while larger numbers 9.0/50.8 nm are observed for sample B. Similar dot densities 1.62 and 2.43 $10^{10}\ cm^{-2}$ are observed for samples A and B, respectively. Although in theory, QDs are of zero volume and three-dimensional quantum confinements are expected, nm-size heights with several tens of nm diameters are commonly observed for common QD structures. In the case of samples

a)Electronic mail: shihyen@gate.sinica.edu.tw.

TABLE I. The wafer structures of the sample A, B, and C.

	Samples	A	B	C
	Top Contact	300 nm GaAs $n = 2 \times 10^{18}$ cm^{-3}		
10 x	42 nm GaAs	Undoped		
	8 nm $In_XGa_{1-x}As(X=)$	0.15		
	InAs QD Layer (ML)	2.0	2.8	2.4
	50 nm GaAs	Undoped		
	Bottom Contact	600 nm GaAs $n = 2 \times 10^{18}$ cm^{-3}		
	Substrate	350 μm (100) Semi-Insulating GaAs		

A and B, with increasing InAs coverage from 2.0 to 2.8 ML, the dot height can be one time increase while only ~20% diameter increase is observed. Therefore, the variation of QD height should be the main issue determining its energy levels. The QD height histograms of InAs QDs with the same growth conditions as samples A and B are shown in Fig. 1(b). As shown in the figure, most dot heights of sample A are distributed between 4 and 6 nm, while 7–9 nm is observed for sample B. The results suggest that with increasing InAs coverage, the additional In adatoms would migrate to nearby InAs QDs and undergo nucleation such that larger QDs are observed for sample B.

The normalized 10 K spectral responses of devices A and B at 2.0 V are shown in Fig. 2. As shown in this figure, the peak detection wavelengths of InGaAs-capped QDIPs would shift from 10.4 to 7.6 μm with InAs coverage increased from 2.0 to 2.8 ML. As discussed in the previous report, the intra-band transition between the QD excited state to the quantum-well (QW) ground state of the InGaAs layer is responsible for the observed peak detection wavelength.[7] In this case, with increasing InAs coverage, the increasing dot height as shown in Fig. 1 would lead to the excited state lowering in the InAs QD region. Therefore, with the same InGaAs layers, the energy difference between the QD excited state and the InGaAs QW ground state would be larger for device B than device A. This is the main reason why a shorter peak detection wavelength is observed for device B. The phenomenon of QD height dependent wavelength tuning for the InGaAs-capped QDIPs suggests that if

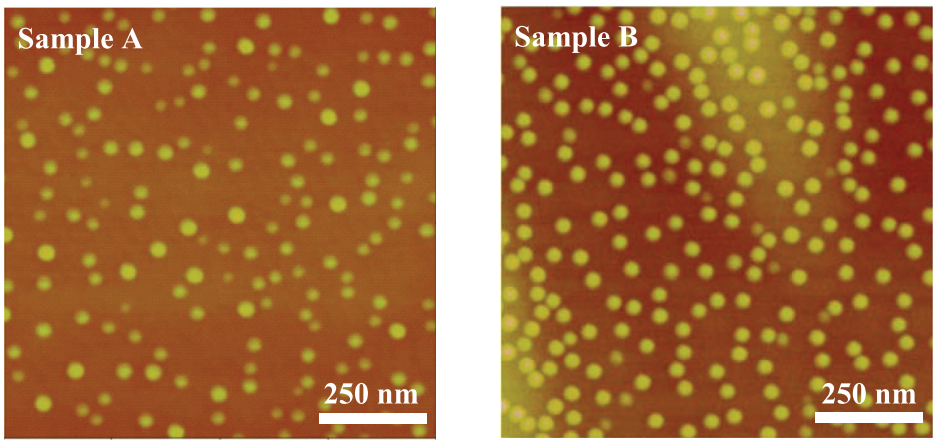

(a)

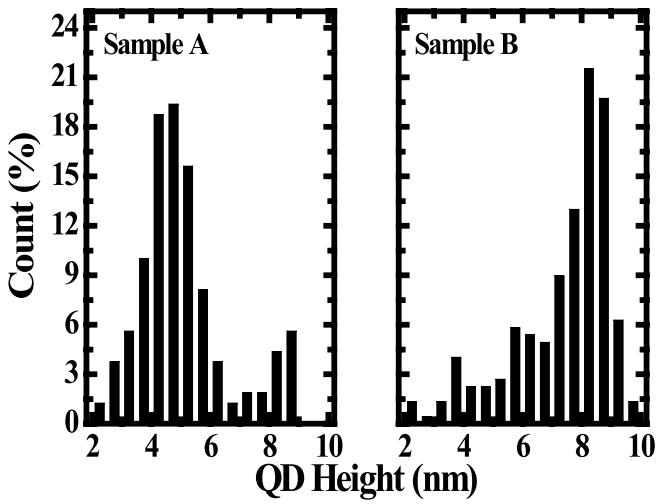

(b)

FIG. 1. (a) The $1 \times 1\ \mu m^2$ AFM images and (b) the dot height histograms of InAs QDs with the same growth conditions as samples A and B.

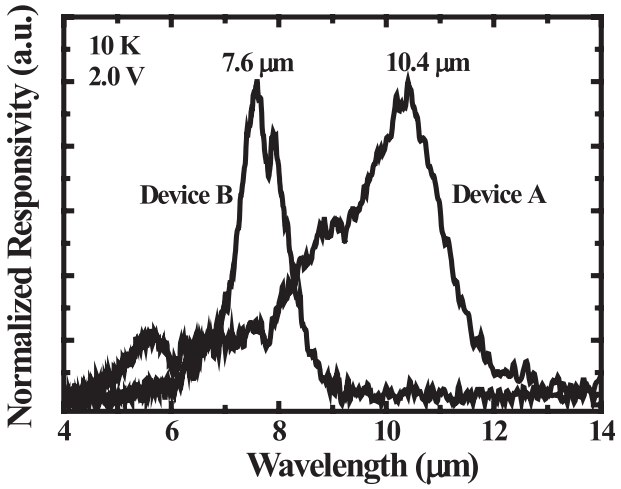

FIG. 2. The normalized 10 K spectral responses of devices A and B at 2.0 V.

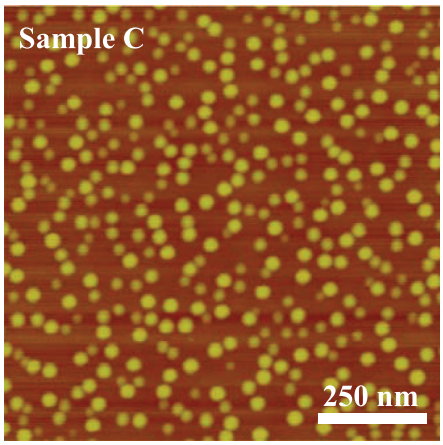

(a)

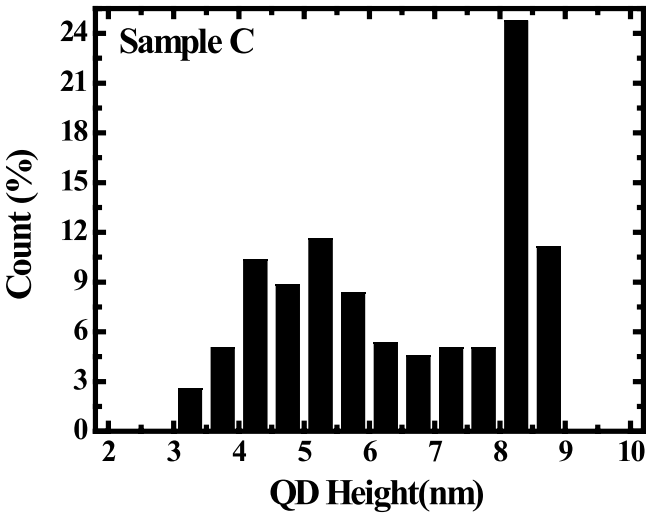

(b)

FIG. 3. (a) The $1 \times 1\ \mu m^2$ AFM image and (b) the dot height histogram of InAs QDs with the same growth conditions as sample C.

a QD layer with bi-modal height distributions can be prepared, a broadband detection covering 6–12 μm may be achieved in a standard QDIP architecture.

With the AFM images shown in Fig. 1 for the QDs with 2.0 and 2.8 ML InAs coverage and the corresponding 10.4 and 7.6 μm responses shown in Fig. 2, it is reasonable to predict that if bi-modal dot heights can be achieved in the same QD layer, which is possible to demonstrate broadband detection. Therefore, sample C with similar wafer structures as samples A and B is prepared. Intermediate 2.4 ML InAs coverage is adopted for the sample. The $1 \times 1\ \mu m^2$ AFM image of the test sample with the same growth conditions as sample C is shown in the Fig. 3(a). As shown in the figure, InAs QDs with bi-modal dot height distribution are obtained. To further investigate the dot height distribution, the dot height histogram is shown in Fig. 3(b). As shown in the figure, bi-modal dot height distributions with one group ranging from 4 to 6 nm and the other from 8 to 9 nm are observed. Since the main issue determining the detection wavelengths is the dot height, the bi-modal dot height distributions of sample C should lead to a broadband detection wavelength with the combination of two different responses.

The normalized 10 K spectral responses of devices A, B, and C are shown in Fig. 4. As shown in the figure, broad detection wavelength from 6 to 12 μm is observed for device C. Since the heights of the two QD groups observed for sample C are close to samples A and B, respectively, the spectral responses have revealed a combination of both devices A and B at the same applied voltage. The results have confirmed that the main issue determining the detection wavelengths of the InGaAs-capped QDIPs is the dot height. Broadband detection can be easily achieved via this structure with broadened dot height distribution.

Since the major application for the QDIPs is on thermal imaging, a single-detector raster scan system is established to demonstrate the possibility of InGaAs-capped QDIPs for this application. The system setup is shown in Fig. 5(a). As shown in the figure, a 20-period InGaAs-capped QDIP with similar structure as device B is mounted on an L-N_2 cooled

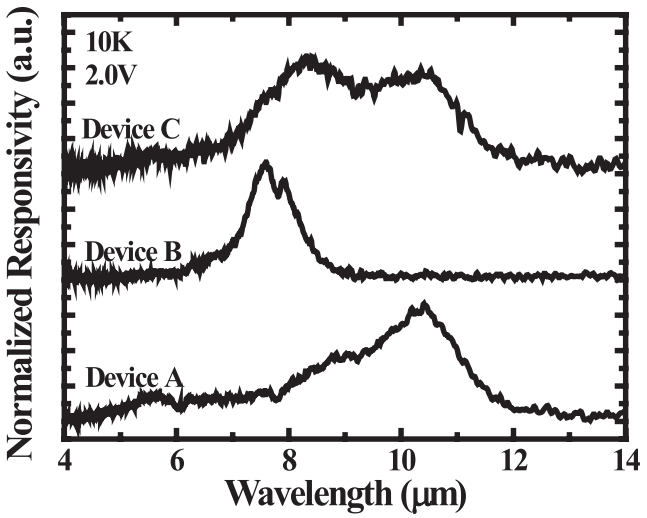

FIG. 4. The normalized 10 K spectral responses of devices A, B, and C at 2.0 V.

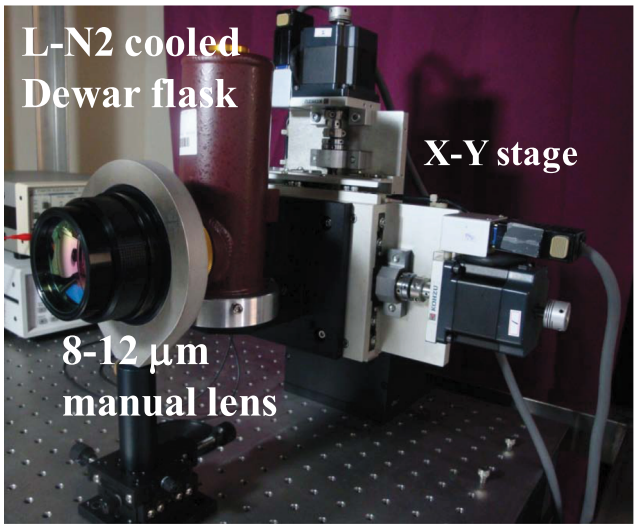

(a)

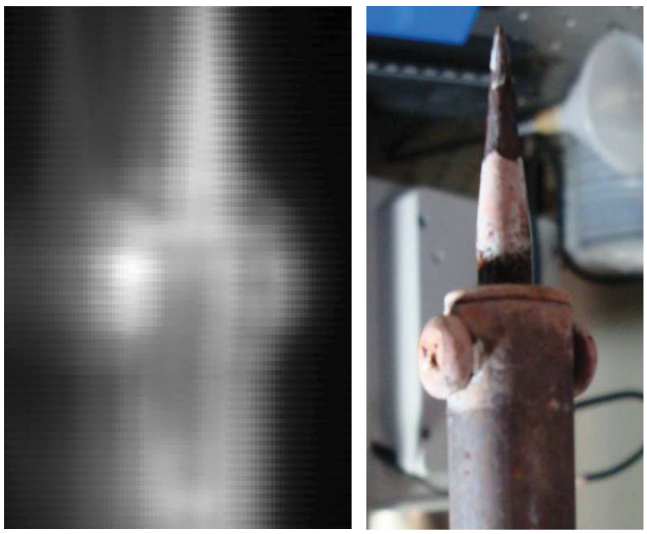

(b)

FIG. 5. (a) The setup of the raster scan system and (b) the scanned thermal image and the picture of the hot solder head.

Dewar flask. With an OPHIR 8–12 μm manual lens with 50 mm focus length and F number 1.0 in front of the device, the single detector is mechanically moved on the focal plane by using a computer-controlled X-Y stage. A Stanford Research SR570 low-noise current preamplifier is used to convert the current signal to voltage and recorded by the computer. With step moving distance of 100 μm in both directions, the thermal image of a hot solder head can be obtained via this approach. The image is shown in Fig. 5(b). For reference, the picture of the solder head is also shown in Fig. 5(b). The results have demonstrated the possible application of InGaAs-capped QDIPs in thermal imaging systems. With the same nature of high-temperature operation and insensitivity to incident light polarization of QDIPs, multicolor and broadband detections can also be achieved by using this structure.

IV. CONCLUSIONS

In conclusion, the influence of QD height distribution on the detection wavelengths of InGaAs-capped QDIPs is investigated. For the device with 2.4 ML InAs coverage, broadband detection combining the responses of the two devices with 2.0 and 2.8 ML InAs coverage are observed. The results have confirmed that the main issue determining the detection wavelengths of the InGaAs-capped QDIPs is the dot height. Broadband detection can be easily achieved via the InGaAs-capped QD structure with broadened dot height distribution. A raster scan thermal image of the InGaAs-capped QDIP has also demonstrated its potential in this application.

ACKNOWLEDGMENTS

This work was supported in part by the National Science Council, Taiwan under the Grant No. NSC 100-2628-E-001-001 and the nano-project by Academia Sinica.

[1]S. F. Tang, S. Y. Lin, and S. C. Lee, Appl. Phys. Lett. **78**, 2428–2430 (2001).
[2]S. Chakrabarti, A. D. Stiff-Roberts, P. Bhattacharya, S. Gunapala, S. Bandara, S. B. Rafol, and S. W. Kennerly, IEEE Photon. Technol. Lett. **16**, 1361–1363 (2004).
[3]S. T. Chou, M. C. Wu, S. Y. Lin, and J. Y. Chi, Appl. Phys. Lett. **88**, 173511–173513 (2006).
[4]S. Y. Lin, Y. R. Tsai, and S. C. Lee, Jpn. J. Appl. Phys., Part 2 **40**, L1290–L1292 (2001).
[5]S. F. Tang, C. D. Chiang, P. K. Weng, Y. T. Gau, J. J. Ruo, S. T. Yang, C. C. Shih, S. Y. Lin, and S. C. Lee, IEEE Photon. Technol. Lett. **18**, 986–988 (2006).
[6]S. D. Gunapala, S. V. Bandara, C. J. Hill, D. Z. Ting, J. K. Liu, S. B. Rafol, E. R. Blazejewski, J. M. Mumolo, S. A. Keo, S. Krishna, Y. C. Chang, and C. A. Shott, Proc. SPIE **6206**, 62060J (2006).
[7]W. H. Lin, K. P. Chao, C. C. Tseng, S. C. Mai, S. Y. Lin, and M. C. Wu, J. Appl. Phys. **106**, 054512 (2009).
[8]W. H. Lin, C. C. Tseng, K. P. Chao, S. C. Mai, S. Y. Lin, and M. C. Wu, IEEE Photon. Technol. Lett. **21**, 1332–1334 (2009).
[9]S. Y. Lin, W. H. Lin, C. C. Tseng, K. P. Chao, and S. C. Mai, Appl. Phys. Lett. **95**, 123504 (2009).